Transport of EOR polymer solutions in low permeability porous media: impact of clay type and injection water composition

Imane Guetni, Claire Marlière, David Rousseau, Manuel Pelletier, Isabelle Bihannic, Frédéric Villiéras

Transport of EOR polymer solutions in low permeability porous media: impact of clay type and injection water composition

Imane Guetni[1,2,], Claire Marliere[1], David Rousseau[1,*], Manuel Pelletier[2], Isabelle Bihannic[2], Frédéric Villiéras[2]*

[1]IFP Energies nouvelles, 1 avenue de Bois Préau, 92852 Rueil-Malmaison, France

[2]Université de Lorraine, CNRS, Laboratoire Interdisciplinaire des Environnements Continentaux, 15 avenue du Charmois, 54500 Vandoeuvre-lès-Nancy, France

*: corresponding authors

KEYWORDS: Porous Media, Low permeability, Enhanced Oil Recovery, Polymer flooding, Retention, Clay

Abstract

The application of polymer flooding for enhanced oil recovery (EOR) to low-permeability porous media (below 100mD) can be very challenging as high polymer retention and poor injectivity are frequently observed. The challenges are mostly related to polymer solutions properties (ionic strength and hardness) and porous media mineralogy (clay content). This paper reports on an experimental study that aims at drawing a better picture of the mechanisms governing the transport of polymer solutions in low permeability clayey porous media. Results confirm the major role played by the injection water composition (salinity and hardness) on polymer conformation and on polymer-minerals interactions. Strong interactions between polymer and clay are also evidenced with significant differences according to the clay type: good propagation and high polymer retention in an uncharged and non-swelling clay (kaolinite) and poor propagation with lower than expected retention in charged or swelling clays (illite, smectite). For kaolinite, the results are interpreted in terms of fast formation of a polymer adsorbed layer on the solids surface whereas, for illite and smectite, they can be explained by the slow diffusion of polymer into clay aggregates, whose presence was evidenced by microscopic analysis. These outcomes stand as new elements for understanding and modeling the transport of polymer solutions in low permeability sandstone reservoirs. They also allow classifying the clays in view of their practical impact on the feasibility of polymer flooding operations.

Introduction

Polymer flooding is now considered as an attractive EOR option for sandstone reservoirs with permeability below 100mD, in particular where lack of gas supply does not allow gas injection. Although several pilots have been performed, difficulties such as high retention of the chemicals, penalizing the economics, and poor injectivity, potentially leading to uncontrolled fracturing, represent serious challenges (Delamaide et al., 2014, Marliere et al., 2015).

Polymer retention increases with the molecular weight of the polymer, with the clay content, with decreasing permeability of the reservoir rock and with decreasing anionic charge of the polymer. Three main mechanisms are classically presented as responsible for the retention of polymer in porous media (Sorbie, 1991)**:**

- Adsorption;
- Mechanical entrapment;
- Hydrodynamic retention.

Adsorption, the most prevalent mechanism in polymer retention, is caused by physical interactions between polymer chains and rock surfaces, such as Van der Waals attraction, electrostatic interaction, and hydrogen bonding. For the main polymers used in polymer flooding applications, adsorption is generally considered as an irreversible process (Lecourtier, Chauveteau, 1984), (Bagassi et al., 1989), (Pefferkorn, 1999) but can vary with the injected polymer concentration ((Zhang, Seright, 2014) ; (Rodriguez Manrique et al., 2014)). Low permeability sandstones are usually rich in clay, which are usually considered as responsible for high polymer adsorption (Green, Wilhite, 2018, Sorbie, 1991).

Mechanical entrapment was studied in particular by Szabo (Szabo, 1975) and Dominguez et al. (Willhite, Dominguez, 1977), who were among the first to study polymer retention in porous media. They concluded that mechanical entrapment resulting from the trapping of large polymer molecules in small pore throats was the most significant retention mechanism and that it was

expected to be even more important in low permeability rocks. Hydrodynamic retention is similar to mechanical entrapment, but is a flow rate dependent effect, meaning that polymer retention increases with the velocity (Chauveteau, Kohler, 1974, Marker, 1973, Willhite, Dominguez, 1977). However, this mechanism is not well understood and is not believed to be a large contributor in field-scale polymer floods (Sorbie, 1991).

Martin (Martin, 1974), in one of the pioneering papers on the use of polymers in low permeability media, recognized the risks of plugging and injectivity issue in low permeability rocks, but he also noted that the pore structure of the porous medium is more important than its actual permeability. This was confirmed by another pioneering work on the subject (Dann et al., 1982). Another work (Vela et al., 1976) showed that the polymer Resistance Factor decreased as permeability increased. Treiber et al. (Treiber, Yang, 1986) concluded that plugging by polymer depends in particular on the permeability of the porous medium and the size of the polymer, and that plugging was unlikely to occur far from the wellbore. For low permeability rocks, low molecular weight polymer should be used as large polymer molecules may not be able to penetrate the lower permeability rocks (Sheng, 2011). This was showed for instance in Daqing (Wang et al., 2009) where the authors determined that the root-mean-square radius of gyration of the polymer should be 5 times less than the pore-throat radius of the reservoir rock. On this basis, in a low permeability range of 5 to 20 mD, polymer molecular weight should be 1.5 to $3x10^6$ g/mol. However, Fletcher et al. (Fletcher, Morrison, 2008) indicated that they were able to inject a $16x10^6$ g/mol molecular weight polymer into a 5 mD core without plugging.

In summary, the existing literature regarding polymer transport in low permeability sandstone rocks show that: (i) retention is higher than in higher permeability rocks and (ii) that the potential injectivity issues can be addressed by reducing polymer molecular weight. However, no study so far have been devoted to finely describing the polymer transport and retention mechanisms in clay-rich low permeability porous media in order to forecast the feasibly (in particular in view of economics) of polymer flooding in reservoirs depending on their mineralogical compositions.

The present work aims at providing elements to draw a better picture of these mechanisms with regard to the nature of the clays and the composition of the polymer injection water. For this purpose, polymer injection (coreflood) experiments were carried out in 4 different types of model granular porous media, made with minerals representative of the typical constituents of low permeability sandstone reservoirs. Namely, these porous media were made of: quartz grains (reference) and mixtures of quartz grains with, respectively, a non-swelling and free of structural charges clay (kaolinite), a non-swelling with structural charges clay (illite) and a swelling clay (smectite). In order to allow comparisons, the porous media were carefully prepared so that they had homogenous permeability and porosity profiles and similar permeabilities within the range 50-100 mD. Their microscopic structures were characterized by SEM.

Coreflood tests have been performed in all 4 types of porous media using solutions of a single polymer type in 3 different injection waters (respectively a low salinity water, a brine with no hardness and a hard brine). The polymer solutions were characterized in terms of intrinsic viscosity and polymer particles size in solution using dynamic light scattering (DLS) and the polymer concentrations were adjusted so that the solutions in the 3 waters had the same viscosity. The coreflood results were analyzed using the conventional petrophysics-related observables for polymer flooding: mobility and permeability reduction factors (also called resistance and residual resistance factors) and polymer irreversible retention.

Materials and methods

For reproducibility reasons, granular porous media of controlled mineralogical composition were used. For each of the mineralogical compositions, polymer solutions prepared in different brines were injected.

Polymer solutions

Salts used in this study for brine preparation are sodium chloride (NaCl) and calcium chloride ($CaCl_2$, $2H_2O$) provided respectively by *Fisher Chemical* and *Merck KGAa*. Salts were first dissolved in distilled water, the solution was then filtered using a cellulose ester Millipore-MF filter of 0.22µm estimated pore diameter and outgassed under vacuum while agitated for at least 30min. Brines can be defined by two parameters: ionic strength I and hardness R^+. Ionic strength evaluates the activity of ions in aqueous solution and it is expressed in mol/L. Hardness is defined as the mass fraction of divalent cations in solution expressed in percentage (%):

$$R^+ = \frac{\sum divalent\ cations}{\sum total\ cations} = \frac{Ca^{2+}}{Na^+ + Ca^{2+}} \qquad \text{(Eq.1)}$$

In the following, brines will be noted SI-R^+. For example, a brine of an ionic strength I=1mol/L and a hardness R^+=20% will be noted S1-02.

In this study, three types of brines were selected, that schematically represent potential injection waters in oilfields:

- A soft brine with very low salinity (NaCl 10^{-3} mol/L): S001-0
- A salted soft brine (NaCl 1mol/L): S1-0
- A salted hard brine: S1-02

For this study, the polymer used is a conventional partially hydrolyzed polyacrylamide (HPAM) Flopaam 3130S provided by *SNF-Floerger*. This polymer is among the EOR polymers with the lowest molecular weight and is hence adapted for applications in reservoirs with

permeability less than 100mD. HPAM solutions were prepared by gradually adding polymer powder to the brine under strong stirring, then left overnight under gentle stirring to allow a good dissolution of the polymer without degradation.

Before their injection in the porous media, polymer solutions were filtered in order to remove debris and microgels. Filtration was carried out under imposed flow rate conditions using a volumetric pump with a polycarbonate membrane with capillary pores from SPI-Pore having a pore diameter of 1µm and at a rate of 70mL/h. Polymer solution viscosity was continuously monitored on-line downstream the membrane during filtration (with a capillary tube – see description below) and compared with the initial viscosity to ensure that the process induces no viscosity loss. As a result, the high shear rate in membrane pores is always shown to be harmless to the polymer.

Characterization

To characterize the fluids, we mainly focused on viscosity measurements.

We used a LS300 viscosimeter developed by *ProRheo* and designed to measure low viscosities at low shear rates. Measurements were conducted using a Couette-like geometry at a temperature of 40°C - which is also the chosen temperature for coreflood experiments. Viscosity measurements consisted in performing, for a duration of 20min, logarithmic shear ramps (ascending then descending in steps) for a shear rate range of 1 to 100 s^{-1}, and measuring corresponding viscosity.

In order to study the conformation of polymer chains in solution, the concept of intrinsic viscosity $[\eta]$ was used. Intrinsic viscosity is expressed in cm^3/g and represents the ratio of the volume swept by the swollen macromolecules over its mass. It can hence be considered as the reciprocal of a "density in solution" (Russel et al., 1989). It can be determined by the Huggins equation which links the reduced specific viscosity $\eta_{spr} = \frac{\eta_r - 1}{c}$ to the intrinsic viscosity as follows

$$\eta_{spr} = [\eta] + K_H[\eta]^2 c + O(c^2) \qquad \text{(Eq.2)}$$

where K_H is the Huggins constant (empirically linked to intermolecular hydrodynamic interactions), c the polymer concentration and η_r the relative viscosity (ratio between the viscosity of the polymer solution $\eta_{polymer}$ and that of the solvent alone η_{brine}).

The intrinsic viscosity can therefore be easily determined experimentally by calculating the limit of the reduced specific viscosity when the polymer concentration tends towards zero:

$$[\eta] = \lim_{c \to 0} \eta_{spr} \qquad \text{(Eq.3)}$$

In addition to viscosity measurements, the hydrodynamic radius R_h of the polymer can be estimated using Dynamic Light Scattering. The technique is based on the fluctuation of the light scattering induced by the Brownian motion of colloidal particles (Russel et al., 1989). Measurements of the light scattered versus time are performed at a given scattering vector $q = (4n\pi/\lambda)\sin(\theta/2)$, θ being the scattering angle, λ the wavelength and n the solvent refractive index. A correlator is used to obtain the autocorrelation function $G(\tau)$ of the fluctuating intensity. For a dilute suspension this function is directly related to the position of the individual particles. If their size distribution is narrow, $G(\tau)$ shows an exponential decay parameterized by a decay rate Γ ; for polydisperse and/or multimodal suspensions, the distribution of Γ values is computed from $G(\tau)$ with numerical algorithms. For $qR_h < 1$ or $qR_h \sim 1$ (low angles), each Γ value is proportional to the translation diffusion coefficient D_0 of particles of a given size. Their hydrodynamic radius R_h is then given by the Stockes-Einstein equation:

$$R_h = k_B T / 6\pi\eta_0 D_0 \qquad \text{(Eq.4)}$$

Where k_B, T, η_0 are respectively Boltzmann constant, absolute temperature and solvent viscosity. It should be noted that for $qR_h > 1$ (wide angles), internal respiration modes affect the determination of Γ which is no longer proportional to the translation diffusion coefficient: as a consequence, the size is underestimated. The experiments were performed using an experimental set-up provided by *Cordouan Technologies*: the sample is illuminated by a laser beam and the intensity of the light scattered by particles in solution over time is collected at a fixed angle (90°) by an Avalanche Photodiode Detector (APD). Three polymer solutions prepared in the three selected brines were characterized at a very low concentration 0.25g/L which is below overlap

concentration C*, in order to be in the dilute regime (a necessary condition for DLS interpretation). Temperature was kept constant at 20°C.

Porous media

In order to study mineralogy effect, three quartz-based porous media having similar petrophysical characteristics with different clays (kaolinite, illite and smectite separately) were used, together with reference porous media made only of quartz.

Minerals

Quartz

In order to obtain granular porous media having a low permeability, a mixture of two types of quartz particles were used. The first one GA39 is a natural sand extracted from Fontainebleau area and provided by *SIFRACO*. It contains about 99% silicon dioxide (SiO_2), its density is 2.65g/m^3 and its average particle size is 100µm. Before use, fines and impurities such as iron (0.2%) were removed from GA39 by performing repeated washes in caustic soda solution (to remove fines by increasing the electrostatic repulsion between fines and particles) and in hydrochloric acid solutions (to dissolve iron impurities). The second sand (BCR-067) is a reference quartz provided by *SIGMA-Aldrich* with an average particle size of about 10µm. BCR-067 is laboratory purity grade as supplied and hence used without further purification.

Kaolinite

Kaolinite $Al_2Si_2O_5(OH)_4$ is the weathering product of feldspars. It has very low surface area and cation exchanging capacity. Due to its uncharged 1:1 layer, strong hydrogen bonds can be formed between the alumina and silica hydroxyl groups of octahedral sheets and tetrahedral sheets of adjacent layers, which is the reason why kaolinite clays are often cited as being non-swelling (Zhang, Cresswell, 2015). The one used in this study is KGa-1 which comes from Washington County, Georgia, USA and is provided by the *Clay Mineral Society (CMS)*.

According to the supplier, KGa-1 stands as a particularly pure kaolinite and was used in this work with no further treatment.

Illite

Illite's general formula is $K_yAl_4(Si_{(8-y)},Al_y)O_{20}(OH)_4$ (usually with $1<y<2$) and is a 2:1 phyllosilicate. Due to possible charge imbalance, Ca and Mg can sometimes replace K. Interlayer cations K prevent the intrusion of H_2O into the structure. Therefore, the illite clays are considered to be non-swelling. The one used in this study is Illite du Puy (I77) provided by *Argile du Velay* and purified before use. The purification consisted in decarbonation using acetic acid to remove carbonates (insoluble in water) followed by repeated washes in caustic soda then in ultrapure water before centrifugation. At the end of the purification process, the clays were lyophilized. The CEC obtained by Le Meur et al. (2019 in preparation) with a similar purified procedure, is 20.3 meq/100g.

Smectite

Smectite's general formula is $(1/2Ca,Na)(Al,Mg,Fe)_4(Si,Al)_8O_{20}(OH)_4nH_2O$. It is an expansible swelling 2:1 phyllosilicate with a permanent layer charge balanced by cations allowing water to enter between the sheets (swelling), inducing reversible cation exchanges and very plastic properties. The measured CEC of the purified sample obtained by Neaman et al. (2003) is 97 meq/100g. The one used in this study is Wyoming montmorillonite (MX80) provided by CETCO France. It was purified before use using the same procedure as for illite.

Porous media: core holder and preparation method

Using those minerals, four different types of porous media were prepared by dry packing the appropriate particle proportions in cylindrical cells made of PEEK having on both ends pistons equipped with Nylon nets with aperture of 10µm (Figure 1). The cells dimensions were 10cm length and 1.5cm diameter. Different intermediate connection taps allow the measurement of differential pressure in the sections 0-1cm; 1-4cm; 4-7cm and the total section 0-10cm, the differential pressure in the section 7-10cm being deduced from the results measured in the other sections. The intermediate pressure taps are connected to differential pressure sensors, of ranges 60, 2500 and 20000 mbar, provided by *ABB*. They were calibrated and adjusted so that there are two sensors of different measurement ranges per section in order to improve the measurements quality and better estimate uncertainties.

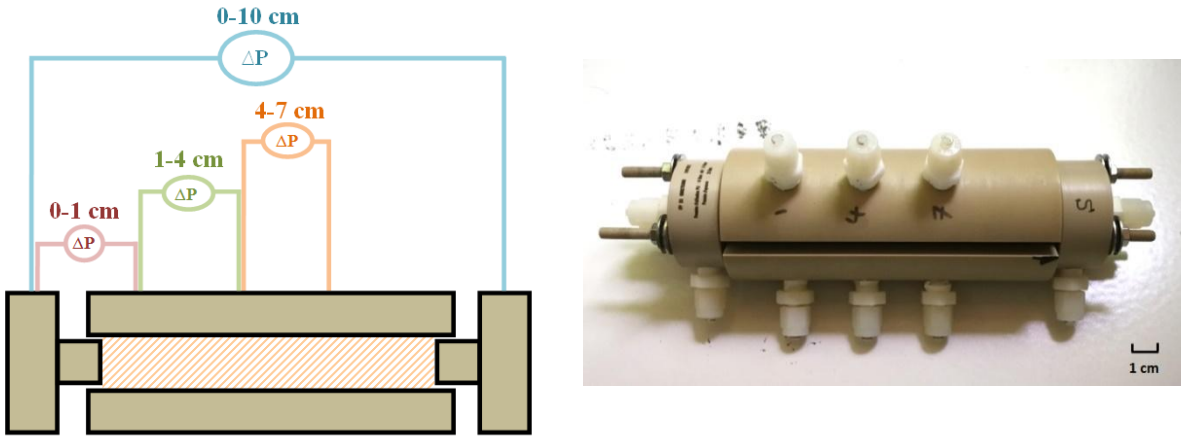

Figure 1: Schematic and illustration of the PEEK cell for granular porous media.

The interests of the intermediate pressure taps layout are first to be able to check for the porous medium homogeneity during permeability measurements, then to follow the progression of the injected fluids front during coreflood experiments and in case of clogging to detect the section presenting the problem.

To study the impact of mineralogy, the proportion of the 3 clays used was set to a fixed value while the quartz proportions were adjusted in order to obtain the expected permeabilities. The

clays particles chosen proportion was 8% in weight, to be representative in terms of order of magnitude of real low permeability sandstone oil reservoirs (Dann et al., 1982; Marliere et al., 2015) while allowing the preparation of homogeneous porous medium (the clay content should not be too high for this purpose). In Table 1 are listed the proportions of quartz used for the different lithologies (labeled, respectively, "quartz", "quartz + kaolinite", "quartz + illite" and "quartz + smectite").

Table 1 : Particles proportions used for the different lithologies

Lithology	Quartz content (wt-%)		Clay type	Clay content (wt-%)
	GA39	BCR-067		
quartz	70	30	/	/
quartz + kaolinite	84	8	**kaolinite KGa-1**	8
quartz + illite	78	14	**illite I77**	
quartz + smectite	86	6	**smectite MX80**	

To avoid particle segregation due to the presence of particles having different sizes and to improve the mixtures homogeneity, a rotary agitator was used. Agitation was maintained for a minimum of 8 hours. The preparation was then put in an oven at 60°C for a minimum of 8 hours to ensure it is completely dry and avoid any humidity effect (capillary bridges between the particles). Quartz and clay grain mixture was then manually dry packed in the cell. The procedure consists of adding progressively a small amount of the mixture and vibrating the cell after each addition by tapping it using a wooden stick.

Characterization

Characterization of porosity and pore volume

Porosity and pore volume (PV) of the porous medium, were determined by gravimetry and tomography.

For gravimetry, the mass and dimensions of the cell were simply determined before and after the porous medium packing, which allows calculating porosity ϕ(%) and pore volume PV (mL) of the porous medium.

Computerized Tomography scan (CT-scan) was used to provide the porous medium porosity profile and an estimation of its average porosity. Using a medical scanner Discovery 750HD provided by *GEHD*, the procedure consists of scanning the cell with an X-ray beam, after which a detector measures the transmission which varies depending on the density of the passed through material. During this process, the cell is automatically moved in order to scan all the sections, and the reconstruction of the obtained images constitutes the spectral profile. The porosity profile is then obtained by the use of a correlation based on two coefficients which are determined by analyzing the spectral profiles and porosities of reference porous media.

An example of the porosity profile using CT-scan obtained for a porous medium containing quartz only is given in Figure 2. Obtained results give the mean porosity and show the overall homogeneity of the porous medium. The corresponding mean porosity is: $\phi_s = 30 \pm 1\%$ which is in good agreement with the porosity determined by the gravimetric method: ($\phi_g = 32 \pm 1\ \%$).

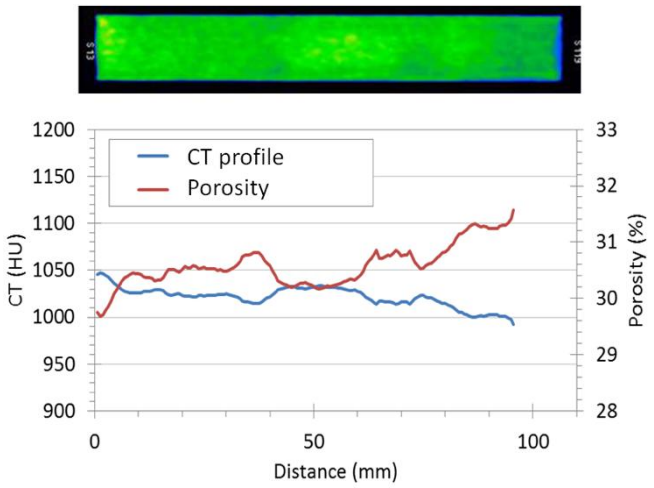

Figure 2: Porosity profile and CT-scan image of the quartz only porous medium.

Determination of permeability

For the four studied porous media, quartz content was adjusted in order to obtain a permeability around 50-100mD.

For permeability determination, the porous medium was first saturated with brine (solvent of the polymer solution to be injected in the medium). After that, the injection rate was increased then decreased over a range of injection rates from 0.8 to 150mL/h, while keeping each injection rate long enough to achieve the differential pressures stabilization in the different sections of the porous medium.

Three cycles of increasing then decreasing flow rates were performed in order to obtain a reproducible and relatively uniform permeability profile. Indeed, as high injection rates can potentially change the granular porous medium structure by inducing particle displacement, this three cycles method allowed ensuring that the granular pack was fully stabilized and homogeneous. In addition, a *Millipore* filter of 0.22µm pore diameter was placed downstream of the porous medium and connected to pressure sensors to ensure that there is no pressure increase that would indicate accumulation of fine particles coming from the porous medium. An example of the permeability profiles obtained during the three cycles is given in Figure 3 for the quartz only porous medium with S1-0 brine.

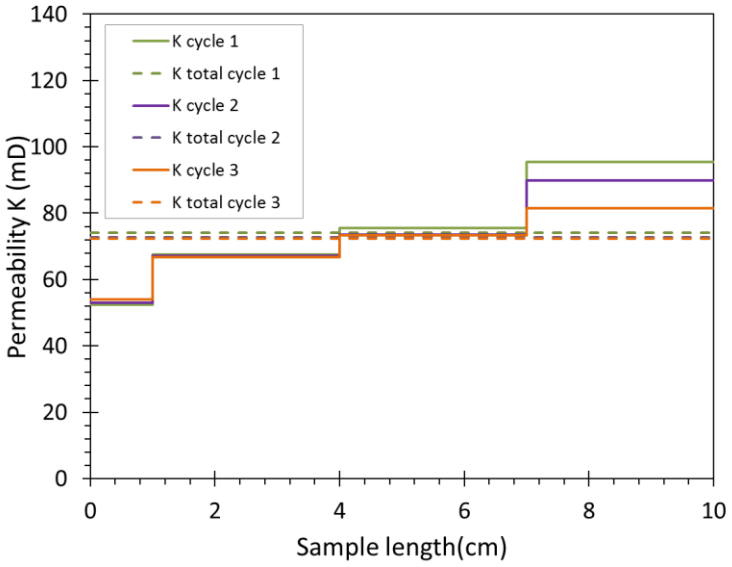

Figure 3: Permeability profiles for the quartz only porous medium with S1-0 brine.

This Figure shows that the sections (0-1cm) and (7-10cm) have permeabilities that are respectively lower and higher than the mean permeability value, which is probably due to the packing procedure. Nevertheless, the porous medium is globally homogeneous, with no remarkable differences between the three permeability cycles except for the last section. The corresponding mean final permeability is around $k = 72 \pm 4$ mD.

In Figure 4 are presented the final permeability profiles of the different studied porous media which shows that they are all in the range of the fixed permeability (50-100mD).

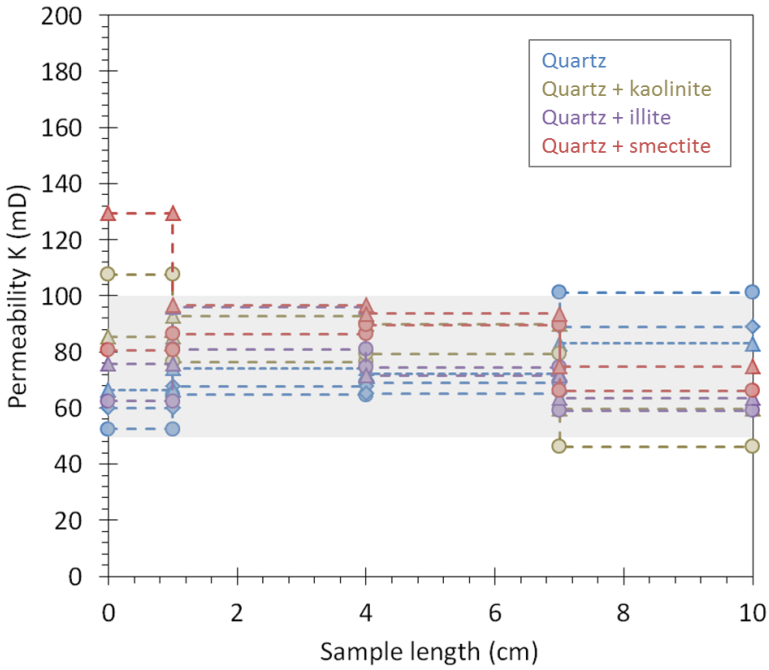

Figure 4 : Permeability profiles of the 4 types of porous media

Textural characterization: specific surface area determination

The determination of the specific surface area was done via physical adsorption of nitrigen at liquid nitrogen temperature. The measurement was carried out using point by point manometry, on a BElSORP II device provided by *BEL JAPAN*. The specific surface area of studied samples was estimated from the amount of nitrogen adsorbed regarding its pressure at the boiling temperature of liquid nitrogen and under atmospheric pressure. The isotherms obtained were then analyzed according to the Brunauer, Emmett and Teller (BET, (Brunauer et al., 1938)) model for the specific surface area estimation, and by applying the De Boer t-plot model (Mikhail et al., 1968) for the accessible microporosity to nitrogen.

Results obtained from specific surface area measurements are summarized in Table 2 for the different minerals and mixtures used in this study. Quartz present very low values of specific surface area compared to clays, with illite having higher specific surface area than kaolinite and smectite.

Table 2 : Results obtained from specific surface area measurements

		Specific surface area (m^2/g)
Minerals	GA39	0.08 +/- 0.05
	BCR067	0.60 +/- 0.1
	KGa-1	7.80 +/- 0.2
	I77	128.0 +/- 0.5
	MX80	46.0 +/- 0.2

Textural characterization: scanning electron microscopy (SEM) observation

Scanning electron microscopy (SEM) is a microscopy technique allowing the visualization of samples' surface and shape. This technique was used as a part of porous media characterization to visualize their shape and structure, evaluate their homogeneity and get an idea about the organization of particles of different size. The electron beam scans the sample's surface which retransmits some electrons, then a detector synchronously captures the signal induced by this beam to form a reconstructed image, which is the cartography of that signal.

The preparation of the sample of granular porous media for SEM analysis involves several steps: sampling, lyophilization, resin impregnation, cutting, grinding and finally polishing. The sample was extracted at the end of the coreflood experiment using a copper tool with a diameter around 0.7cm. It was sampled by slow rotation of the copper tool to preserve as best as possible the medium structure. Once extracted, the sample was lyophilized (rapid freezing at -80°C followed by a complete vacuum dehydration of the sample to preserve its structure).

The sample was then impregnated with a mix of resin and hardener, placed under vacuum for about 20min then left to dry in open air for a minimum of 48hours. After hardening, the sample was cut and ground in order to obtain a flat surface. It was then gradually polished with Silicon Carbide (SiC) abrasives with grains size from 15µm to 1µm. The surface was observed at each polishing step using a binocular microscope: polishing is completed when no more scratches are

visible on the sample's surface. Finally, a metallization was performed: a thin carbon layer was deposited on the sample's surface using an evaporator metallizer. For results analysis, obtained images ware processed using *JMicroVision* or *ImageJ* softwares.

Summary: main properties of the porous media

Table 3 summarizes the characteristics of studied porous media. It shows that obtained permeabilities were all in the chosen permeability range. The values of specific surface area presented in the table were measured from porous media just after been manually dry packed in the cell. Results obtained are in good agreement with a the calculated specific area based on the measurements given for each mineral in Table 2 and the minerals proportions presented in Table 1.

Table 3 : Summary of the characteristics of studied porous media

Porous medium	**Brine**	**Porosity (%)**	**Permeability (mD)**	**Measured specific surface area (m^2/g)**	**Calculated specific surface area (m^2/g)**
Quartz	S001-0	31.4	71	0.20	0.24
	S1-0	31.0	72		
	S1-02	31.9	75		
Quartz + kaolinite	S001-0	31.0	52	0.73	0.72
	S1-0	31.1	66		
	S1-02	31.3	78		
Quartz + illite	S1-0	29.8	69	10	10.4
	S1-02	29.5	75		
Quartz + smectite	S1-0	32.4	80	3.6	3.6
	S1-02	33.1	90		

As it can be seen on Table 3, very similar petrophysical characteristics for all the porous media were achieved using this method - in our case, a permeability around 50 – 100 mD. However, for porous media with clay, a change in permeability has been observed depending on the brine used. As shown in Table 3, a slight change in permeability was observed for lithology 2 (with kaolinite content) as the permeability is lower with decreasing salinity. For the third and fourth lithologies – with illite and smectite content, it was not possible to carry out the experiment using the brine S001-0 as the permeabilities obtained were very unstable and of values below 6mD resulting in a permeability decrease of around 90%. These results are not surprising and are consistent with clay dispersion and/or pore bridging usually observed with low salinity brines.

Coreflood setup and procedure

Experimental setup

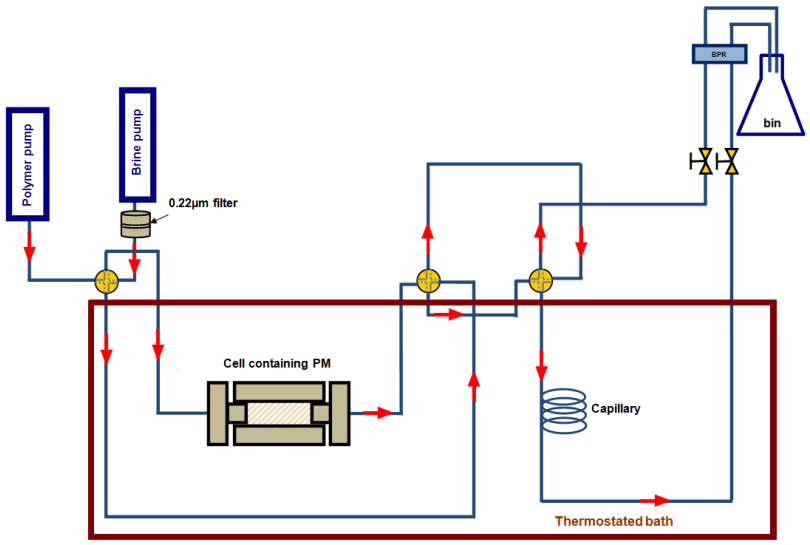

Figure 5 : Schematics of the experimental set-up for coreflood tests.

The experimental set-up (Figure 5) used for this study, consists of two double cylinder Quizix QX6000 pumps provided by *Chandler Engineering*: one for polymer solutions and one for brines. The latter was equipped with a 0.22µm Millipore filter at its outlet used to remove possible impurities in the injected brine. A capillary tube with a diameter of 500µm and a length of 1.5m and a by-pass were respectively

used to measure polymer viscosity and to bypass the porous media. Two pressure sensors were connected to the capillary tube for viscosity measurements. All experiments were performed at 40°C by the use of a temperature-regulated bath, composed of a water tank and a heating coil for temperature regulation. In order to limit evaporation, plastic balls were placed on the water surface.

Injection protocol

In order to simulate in-depth flow in an oil reservoir during EOR operations, the injection rate chosen for this study was set at 0.8ml/h, corresponding to an interstitial velocity of 0.3m/day and an estimated shear rate of $20s^{-1}$ for a permeability around 100mD.

For polymer corefloods, polymer injection was performed in typically two stages ("two slugs method"). Initially, the porous medium was saturated with the brine to be used in each given experiment. A polymer slug at the same salinity was first injected until the stabilization of the differential pressures, followed by a brine injection to displace the polymer retained reversibly. Then, a second polymer slug was injected. At the end of the second slug, the injection rate was increased up to 30 mL/h and then stepwise decreased in order to simulate the velocities around injection wells. Brine was finally injected until differential pressure stabilization, and the same series of injection rate variation was then applied for the brine. During the injection process, the polymer's viscosity was monitored before each slug using the capillary tube, in order to detect the polymer breakthrough and to make sure the polymer was not degraded over time.

Observables

The observables of all experiments were differential pressures, normalized as mobility reduction factors and permeability reduction factors. mobility reduction factor (or resistance factor), R_m, is directly derived from the readings of the pressure drop:

$$R_m = \frac{\Delta P_{polymer}}{\Delta P_{ref\ brine}} \qquad \text{(Eq.5)}$$

$\Delta P_{refbrine}$ being the pressure drop during the brine injection before polymer injection and $\Delta P_{polymer}$ the pressure drop during polymer injection at the same injection rate. R_m can be determined for

each individual section of the porous medium over which the pressure drop is determined. According to Darcy law, R_m corresponds to the ratio between the brine mobility $(k/\eta)_{brine}$ and that of the polymer solution $(k/\eta)_{polymer}$. R_m is obviously associated to the polymer's apparent viscosity in the porous medium and represents the product of the apparent viscosity and a permeability reduction factor.

The part of the polymer irreversibly retained in the porous medium induces an "irreversible" permeability reduction that is represented by the permeability reduction factor (or residual resistance factor) R_k, defined as the ratio between the reference permeability of the medium $k_{reference}$ and its permeability after polymer injection $k_{post\text{-}injection}$

$$R_k = \frac{k_{reference}}{k_{post-injection}} = \frac{\Delta P_{post-injection}}{\Delta P_{refbrine}} \qquad \text{(Eq.6)}$$

$\Delta P_{refbrine}$ and $\Delta P_{post\text{-}injection}$ being respectively the pressure drop during brine injection before and after polymer injection.

Considering the porous medium to be a bundle of capillaries all of radius r_h (r_h standing for an estimation of the pore throat's hydrodynamic radius), and if the structure of the pours medium is not altered by the injection of the polymer, an adsorbed layer thickness ε_h can be determined from the permeability reduction according to:

$$\varepsilon_h = r_h\,(1 - (R_k)^{-1/4}) \qquad \text{(Eq.7)}$$

where r_h writes

$$r_h = \alpha(8k/\phi)^{1/2} \qquad \text{(Eq.8)}$$

k being the initial permeability of the porous medium, ϕ its porosity and α a prefactor that has been determined by Chauveteau (Chauveteau, 1981) and found equal to 1.15 for granular porous media.

The two slugs method allows estimating the irreversible polymer retention in the porous medium by analyzing the successive breakthroughs of the two polymer slugs by the use of the capillary tube placed at the outlet of the porous medium.

As shown schematically in Figure 6, polymer irreversible retention $\Gamma_{retention}$, (expressed in µg/g: micrograms of polymer retained per gram of rock) is quantified based on the shift between

the injected polymer volumes at breakthrough of the first and the second slug respectively V_{BT1} and V_{BT2} ((Dawson, Lantz, 1972)):

$$\Gamma_{\text{retention}} = (V_{BT1} - V_{BT2}) * C_{pol}/m_{MP} \qquad \text{(Eq.9)}$$

with C_{pol} and m_{MP} being respectively the polymer concentration and the mass of porous medium.

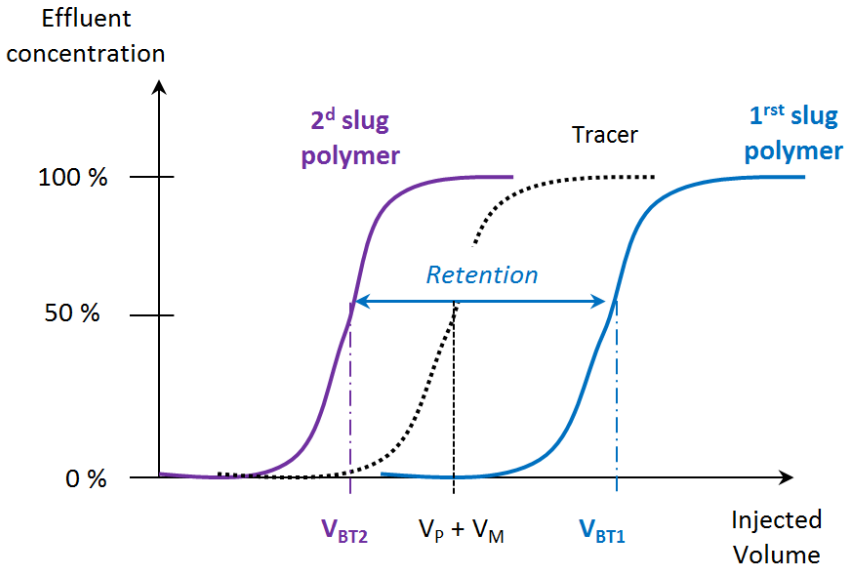

Figure 6 : Schematic of the two slugs method breakthrough curves for retention determination.

It is important to note that in most cases, where no plugging occurs, retention is often associated with adsorption considered to be its major component.

Results and discussion

Polymer solutions

Before selecting the brines to be used in coreflood experiments, a viscometric study was carried out using brines of various ionic strengths and hardnesses and different concentrations.

It should first be stressed that, due to the relatively low molecular weight of the polymer investigated, all polymer solutions have been shown to be Newtonian over the range of shear rate investigated (1 to 100 s^{-1}). The viscosity results presented and discussed in the following should hence be understood as viscosities on the Newtonian plateau. The results obtained in terms of relative viscosity η_r as a function of polymer concentration are shown in Figure 7. Apart from the classical increase of viscosity with concentration, we notice that the polymer viscosity decreases with increasing salinity and hardness, which is the usual consequence of charge screening effects. In other words, the polymer concentrations required to achieve the same relative viscosity are higher for high values of ionic strength and hardness.

Intrinsic viscosities $[\eta]$ were derived from the viscosity measurements in order to study the polymer chains "density" in solution with regard to ionic strength and hardness. Results versus ionic strength and hardness on intrinsic viscosity are presented in Table 4 and also, respectively, in Figure 8 (a) (intrinsic viscosity versus. ionic strength for fixed hardnesses) and Figure 8 (b) (intrinsic viscosities versus hardness for fixed ionic strengths).

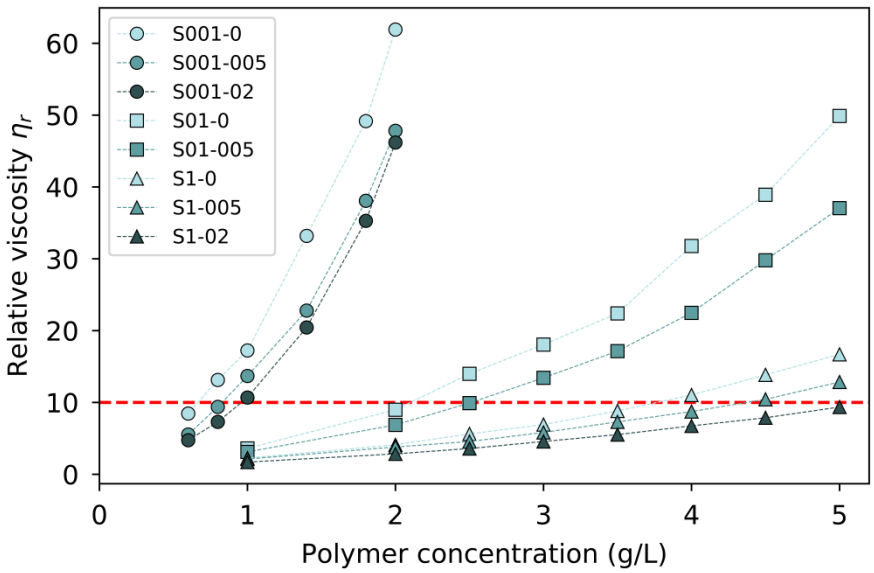

Figure 7 : Relative viscosity as a function of polymer concentration for used brines. The red line being the relative viscosity used for coreflood experiments.

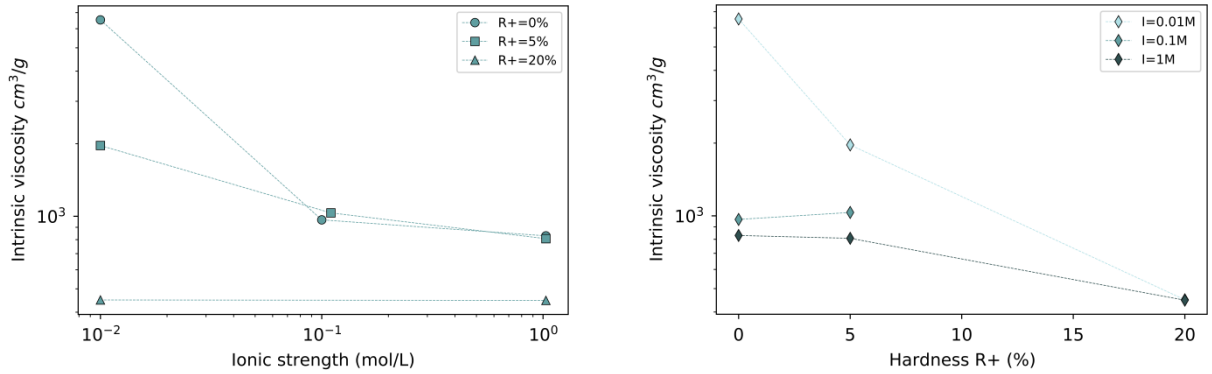

(a) (b)

Figure 8 : Intrinsic viscosity vs. (a) ionic strength for fixed hardnesses and (b) hardness for fixed ionic strengths.

We observed that increasing the ionic strength with fixed hardness as well as increasing the hardness with fixed ionic strength induces a decrease in intrinsic viscosity. These results are

expected as the added salt screens the polymer side chains charges which leads to a decrease in hydrodynamic volume, meaning a higher "density" and thus a lower intrinsic viscosity (intrinsic viscosities from 6530 cm^3/g in S001-0 to 830 cm^3/g in S1-0). In the case of increasing hardness, the screening effect was even more significant (830 cm^3/g in S1-0 to 450 cm^3/g in S1-02) as the divalent cations bind more tightly to the polyelectrolyte due to their double charge (bridging effect) and polarizability which results in denser polymer chains (Sheng, 2011).

For the subsequent assays (in particular coreflood tests), only the three above-mentioned brines (S001-0, S1-0 and S1-02) will be investigated. Furthermore, it was decided to set a fixed relative viscosity for each polymer solution investigated ($\eta_r \approx 10$) in order to assess for the impact of brine composition in conditions representative of typical field application of polymer flooding. Accordingly, polymer concentrations were adjusted to meet this ratio depending on the brine type as shown in Table 4.

Table 4 : Summary of the characteristics of selection polymer solutions for corefloods.

Brine	**Ionic strength (mol/L)**	**Hardness (%)**	**Total salts (g/L)**	**Polymer concentration corresponding to $\eta_r = 10$**	**Intrinsic viscosity [η] (cm^3/g)**	**K_H**
S001-0	0.01	0	0.6	0.7	6530 ± 400	0.24
S1-0	1.03	0	60	3.8	830 ± 45	0.57
S1-02	1.03	20	57.2	5.2	450 ± 15	1.21

Discussion on the intrinsic viscosities have to be confronted to the DLS measurements. DLS results always indicated that hydrodynamic sizes of the solutes were roughly of the order of 300 nm, but unfortunately, due to the polydispersity in size of the polymer solutions, they cannot be translated in precise hydrodynamic sizes. They can however be discussed using the raw autocorrelation functions. As shown in Figure 9, a shift towards higher decay rates is clearly

observed when the salinity was increased from S001-0 to S1-0. This corresponds to larger diffusion coefficients and hence to smaller hydrodynamic sizes and is consistent with a higher "density" in solution of the chains in S1-0 than in S001-0. When hardness is increased from S1-0 to S1-02, on the contrary, a shift towards larger hydrodynamic sizes is observed. This is in apparent contradiction with the decrease in intrinsic viscosity suggesting higher density. The results can be reconciled considering the values of the Huggins constant (K_H). As reported in Table 4, K_H. significantly increases from S1-0 ($K_H = 0.57$) to S1-02 ($K_H = 1.21$). This suggests that attractive interactions between chains exist in the hard brine (likely because of the cationic bridging effect entailed by the divalent cations). Eventually, the viscosity and DLS results suggest that, in S1-02, solutes made of multiple, but dense, polymer chains are present.

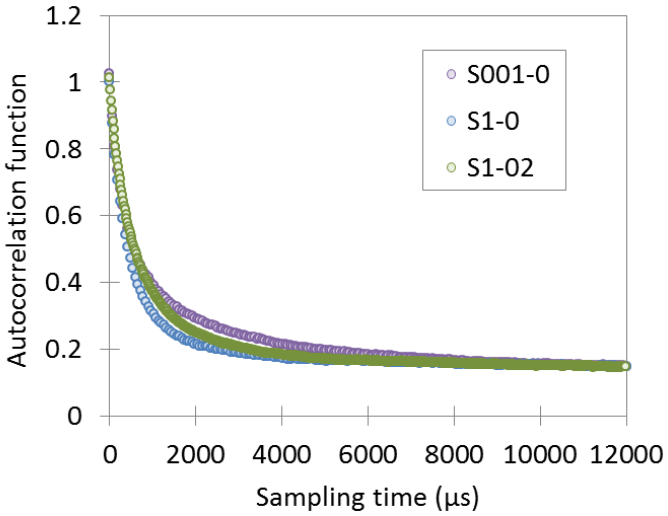

Figure 9 : Autocorrelation function versus sampling time from DLS measurements

Microscopic structure of the sand and clays packs

SEM experiments were carried out in order to investigate the structure of the porous media and assess for their homogeneity. The results are presented in Figure 10 for a view of the quartz only porous media and on Table 5,

Table 6 and Table 7 for comparisons between the quartz only porous media and, respectively, the quartz and kaolinite, quartz and illite and quartz and smectite porous media.

As a general outcome, all SEM observations confirmed the homogeneity of the porous media. The case shown on Figure 10 stands as a good example for this: by analyzing the SEM image, the calculated proportions, 70% for GA39 and 30% of BCR-067, were found in agreement with the proportions used in the mixture (Table 1) and a good spatial repartition at pore scale of the small particles towards bigger sand grains was also observed. The other SEM images presented and discussed in this section can also be considered as representative of the structure of each porous medium.

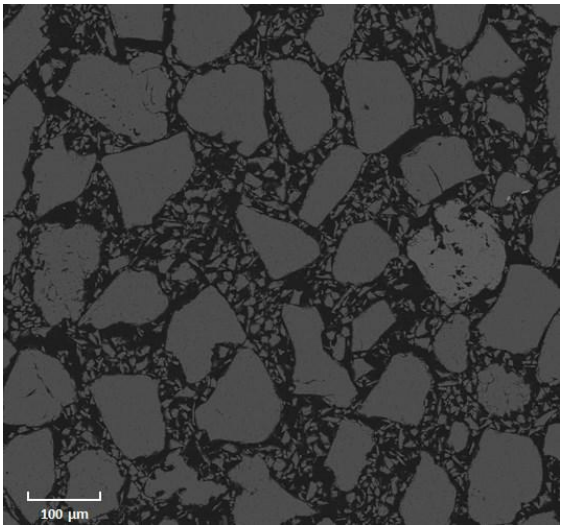

Figure 10 : SEM image obtained for a quartz-only porous medium (MP 1-2, brine S1-0)

The images corresponding to the quartz and kaolinite porous medium (Table 5) show that kaolinite grains are smaller than quartz grains and that they are well separated. No changes have also been observed with regard to salinity, as in low (S001-0) and high (S1-02) salinities the porous media structures are similar. This observation is not surprising as kaolinite grains are not particularly charged in our experimental conditions.

For porous media containing illite, images of Table 6 show that, unlike kaolinite, illite was strongly affected by salinity. In low salinity (S001-0), because of the non-screened interactions

between the clay grains, unstable illite filament-like structure were formed. This resulted in reducing drastically the permeability and impairing the mechanical stability of the granular packs. As a consequence, it was not possible to carry out polymer injection experiments in S001-0 in presence of illite. For the higher salinities (S1-0 is shown as an example but the observed structure was similar in S1-02), conversely, illite aggregates were formed with a size close the quartz grains and the granular packs were found to be stable. Polymer injection experiments could hence be performed.

For the porous media with smectite (Table 7) similar observations as for illite were made, with the same practical consequences (namely it was not possible to perform polymer injection experiments in S001-0). However, the smectite aggregates observed in high salinity conditions included micron-size voids which made them potentially more accessible to polymer than the illite aggregates.

Table 5 : Comparison between SEM images of quartz only and quartz + kaolinite porous media.

Quartz	Quartz + kaolinite	
S1-0	**S001-0**	**S1-02**
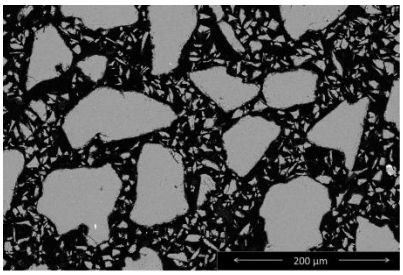	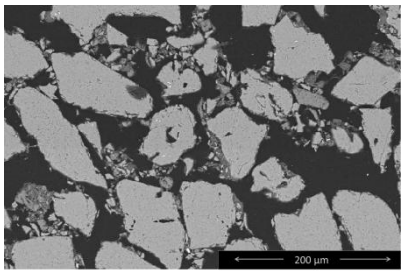	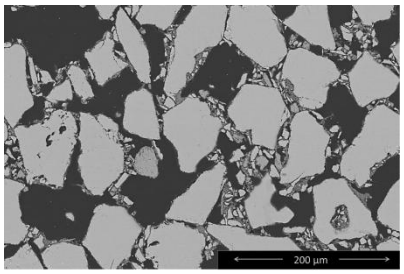
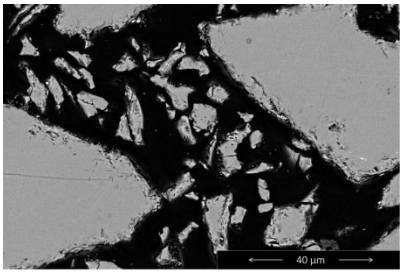	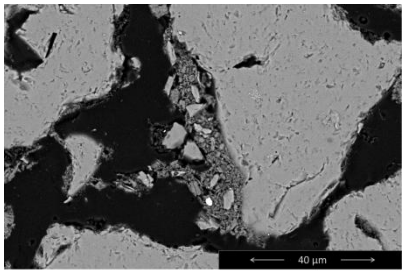	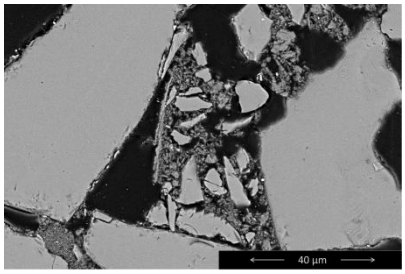
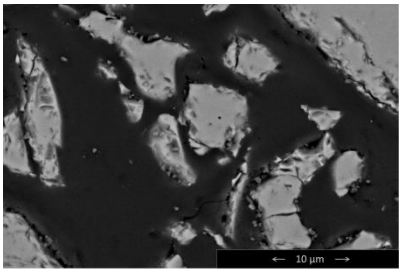	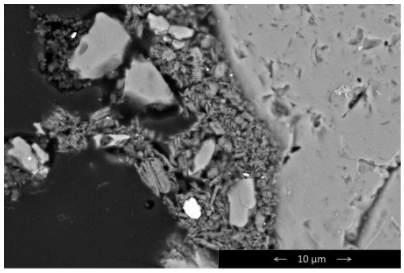	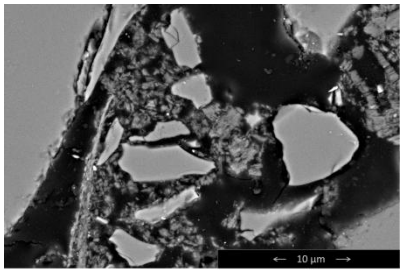

Table 6 : Comparison between SEM images of quartz only and quartz + illite porous media.

Quartz	Quartz + illite	
S1-0	**S001-0**	**S1-0**
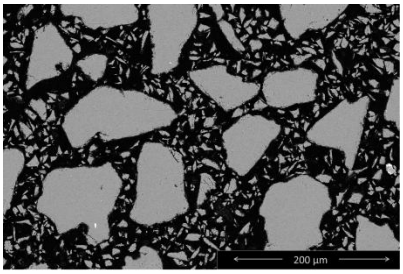	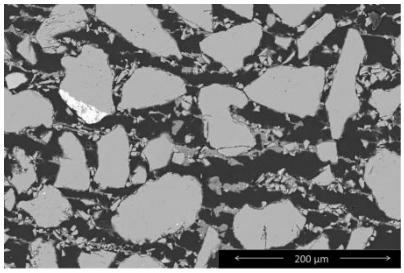	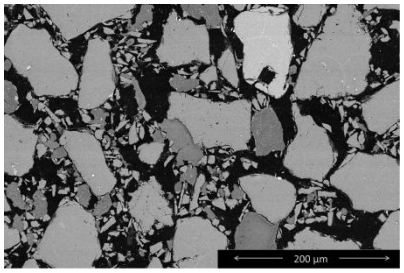
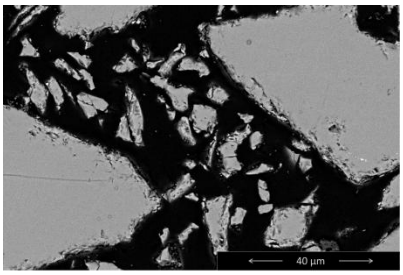	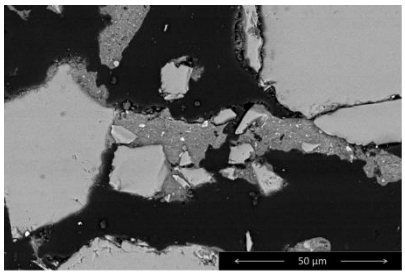	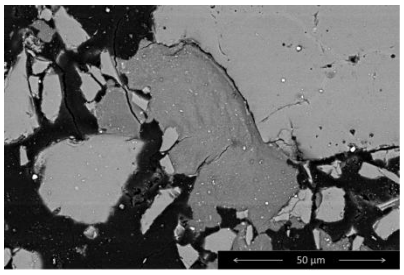
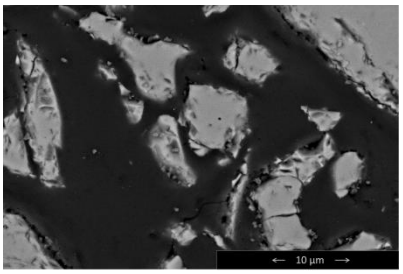	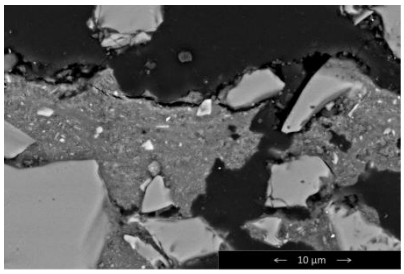	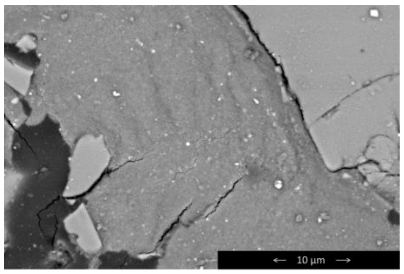

Table 7 : Comparison between SEM images of quartz only and quartz + smectite porous media.

Quartz	Quartz + smectite	
S1-0	**S001-0**	**S1-0**
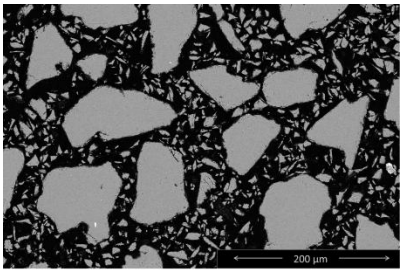	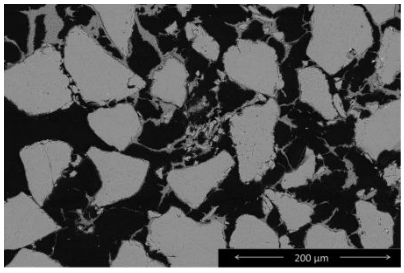	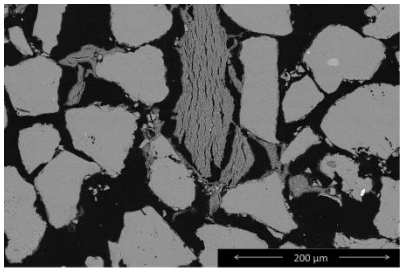
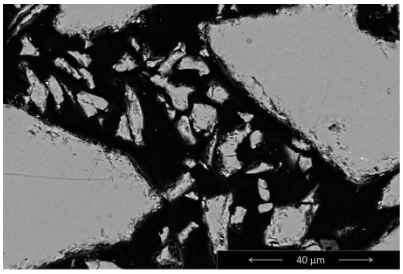	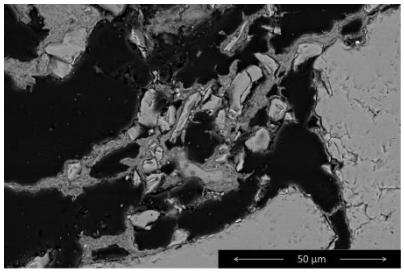	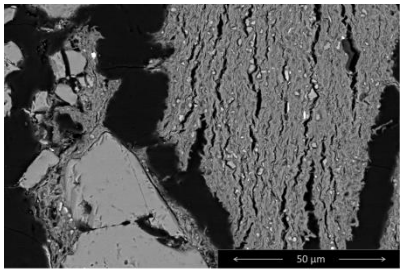
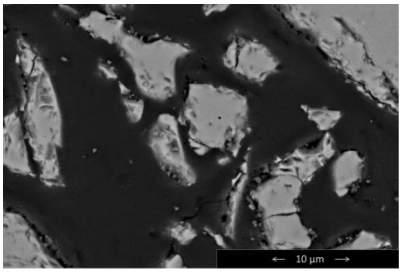	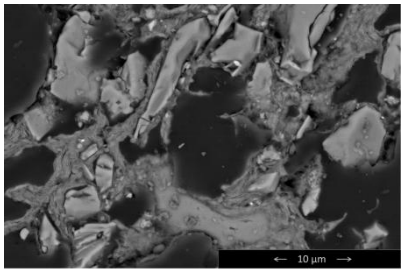	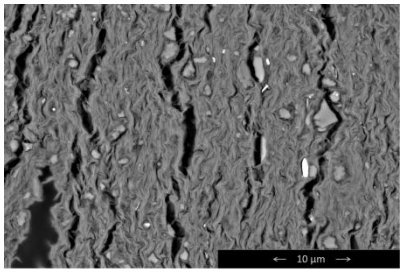

Polymer transport properties

Mobility reductions

The first observables of the polymer injection tests are the mobility reduction factors R_m. For all tests, plots of R_m versus the number of pore volumes of polymer solution injected were analyzed, for each section of the porous media. An example of these curves is given in Figure 11, for the quartz + kaolinite porous media (experiment MP2-2, the R_m curve for the 7-10 cm section is not shown as it is a calculated plot and not a direct experimental measurement). . Similar trends were obtained on the internal sections (1-4 cm and 4-7 cm) for all experiments. In the following, we will present and discuss only results obtained in the intermediate section 4-7cm for the sake of simplicity and because results obtained on this internal section are always representative of the entire porous medium.

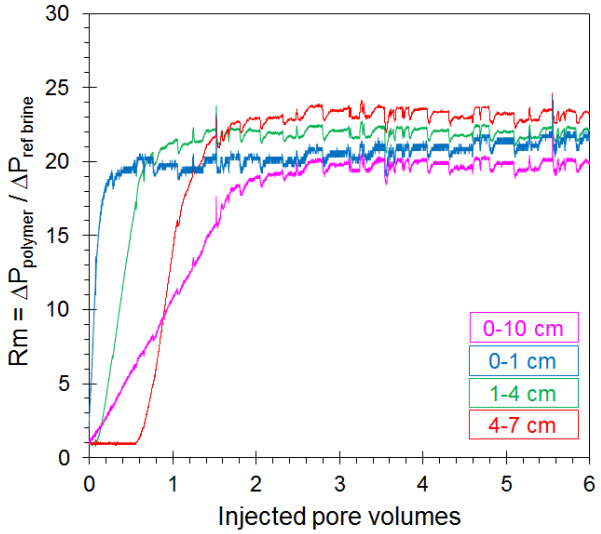

Figure 11 :Resistance factor in different section of MP2-2, brine S1-0.

In Figure 12 and Figure 13 are presented the curves of R_m versus the number of injected pore volumes obtained on section 4-7 cm for the 4 types of porous media and the various brine investigated. From these results, the porous media can be sorted in two groups:

- in the quartz and quartz + kaolinite porous media, R_m increases as a consequence of the propagation of the viscous front with a limited delay due to the retention of the polymer and

stabilizes around 22 ± 2 after less than two pore volumes injected. This fast stabilization suggests that "simple" interaction mechanisms are in play between polymer and solids. Furthermore, the stabilized R_m values do not exceed, depending on the salinities, about two times the relative viscosities of the injected solutions ($\eta_r \approx 10$). This indicates that the permeability reduction entailed by the injection of the polymer is limited to a factor of about two and that no plugging is taking place. In the following, we propose to analyze the results obtained with these two porous media in terms of creation of adsorbed layers of polymers on the grains surface;

- in the quartz + illite and quartz + smectite porous media, the results show much slower stabilization of R_m after the propagation of the viscous front, with increasing trends still observed after 6 pores volumes injected. In addition, for the quartz + illite porous media, the permeability reduction strongly depends on the hardness, with R_m above 40 after 6 pore volumes injected in the S1-0 brine. More complex polymer – solids interactions clearly take place for these two mineralogies. In the following, we propose to analyze the results by focusing on the texture of the sand and clays porous structure.

Irreversible retention and permeability reductions

In Figure 14 are shown the polymer irreversible retentions obtained for the 4 types of porous media and the various brines investigated. These results show that, for all mineralogies, polymer retention increases with increasing both ionic strength and hardness and that the increment is more marked in presence of clays. These expected overall behaviors are the consequence of charge screening effects, cationic bridging between polymer and surface as well as high specific surface area when clays are present.

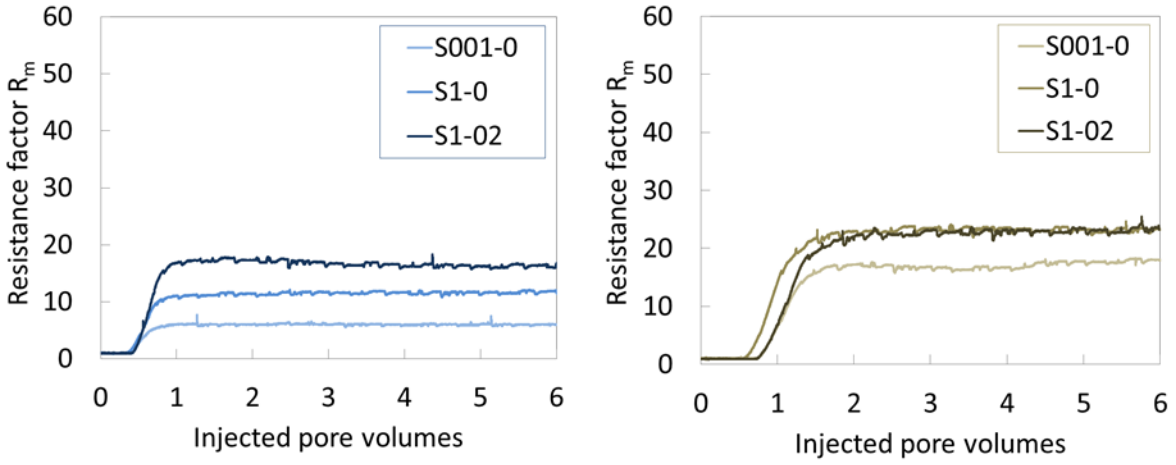

Figure 12: Resistance factor (R_m) on section 1-4 cm versus number of pore volume injected for tests with the brines investigated (S001-0, S1-0 and S1-02) in the quartz porous media (left) and the quartz + kaolinite porous media (right).

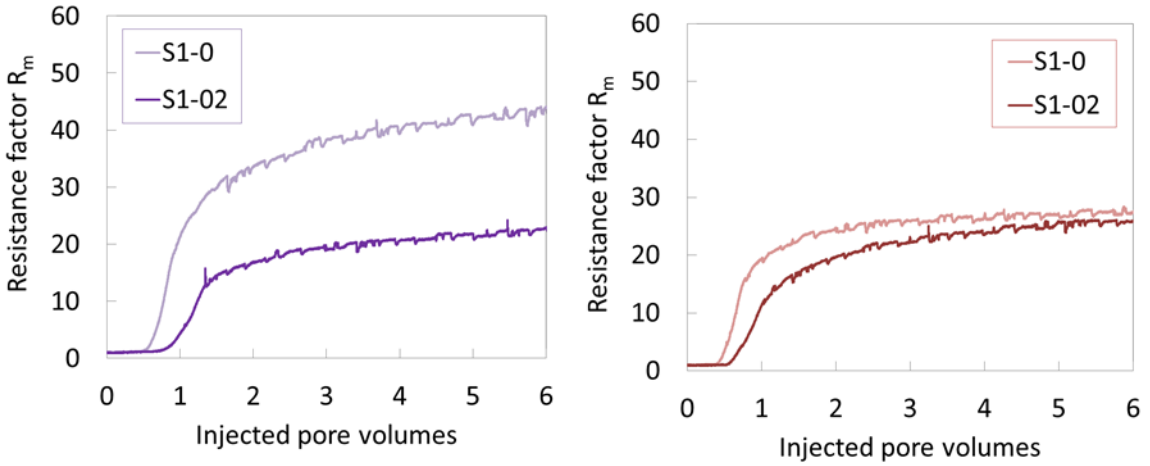

Figure 13: Resistance factor (R_m) on section 1-4 cm versus number of pore volume injected for tests with the brines investigated (S1-0 and S1-02) in the quartz + illite porous media (left) and the quartz + smectite porous media (right).

The main question to address to understand how the polymer was retained in the porous media is the correlation between irreversible retention and permeability reduction. The permeability

reduction factors (or residual resistance factors), R_k, determined for all the experiments performed on the 4 types of porous media in the various salinities are presented in Figure 15.

It appears that for the clay-free porous media, R_k and irreversible retention are straightforwardly correlated, with R_k very close to 1 (namely 1.05, meaning only 5% permeability reduction) in S001-0 increasing to 2.2 in S1-0. For the quartz + kaolinite, a surprising decrease with ionic strength increase is observed. When hardness is increased, R_k increases for all types of porous media, which is consistent with the irreversible retention results. However, the high R_k obtained in the quartz + illite and quartz + smectite porous media (from 6 to 9), compared to the R_k for kaolinite (2 to 4), are unexpected considering that the irreversible retention values are lower in quartz + illite and quartz + smectite than in quartz + kaolinite. This observation is even more surprising when the irreversible retentions are converted from unit mass to unit specific surface area, using the BET data presented in Table 3. The corresponding results are presented in Figure 16 : they show that the polymer irreversible retention per unit specific surface area is much lower in quartz + illite and quartz + smectite than in quartz + kaolinite and even quartz. This obviously means that the specific surface area as determined BET does not correspond to the surface actually accessible to the polymer. To analyze the relation between irreversible retention and permeability reduction, it is usually assumed (Boujlel et al., 2018) that the polymer is retained mainly by adsorption on the porous rock's surface and that the adsorbed layer of polymer reduces the diameter of the pore throats accessible to flow, hence the permeability (this statement leads to Eq. 7, presented above). As, for quartz + illite and quartz + smectite, high R_k are observed together with low surface adsorption, irreversible retention cannot be due, at least mainly, to only a simple surface adsorption in these porous media. This major outcome implies that the main mechanisms for permeability reduction and retention must be different in these mineralogies. It also supports the decision made from the R_m data to apply the adsorbed layer analysis only to the quartz and quartz + kaolinite porous media.

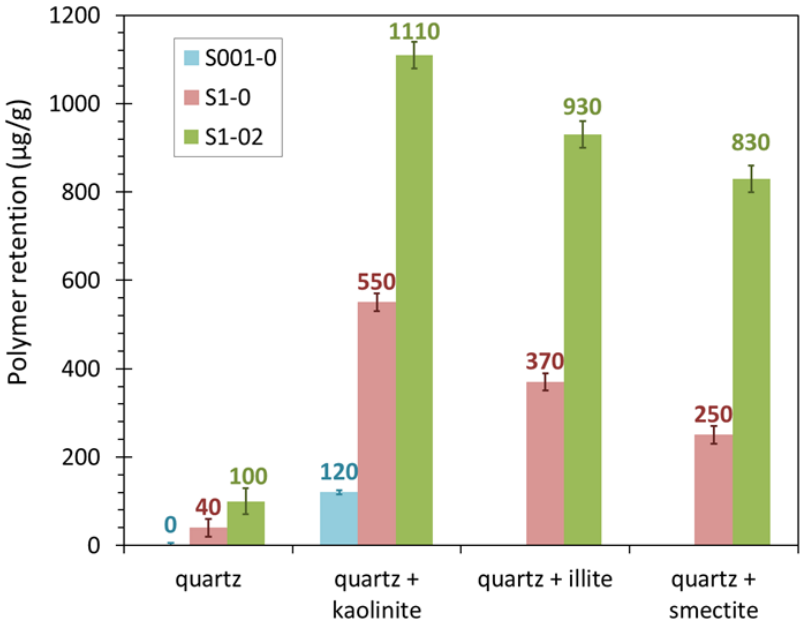

Figure 14: Polymer irreversible retentions (expressed in mass –µg– of retained polymer per unit mass of sand and clays grains –g) determined for the 4 porous media investigated in the various injection brines.

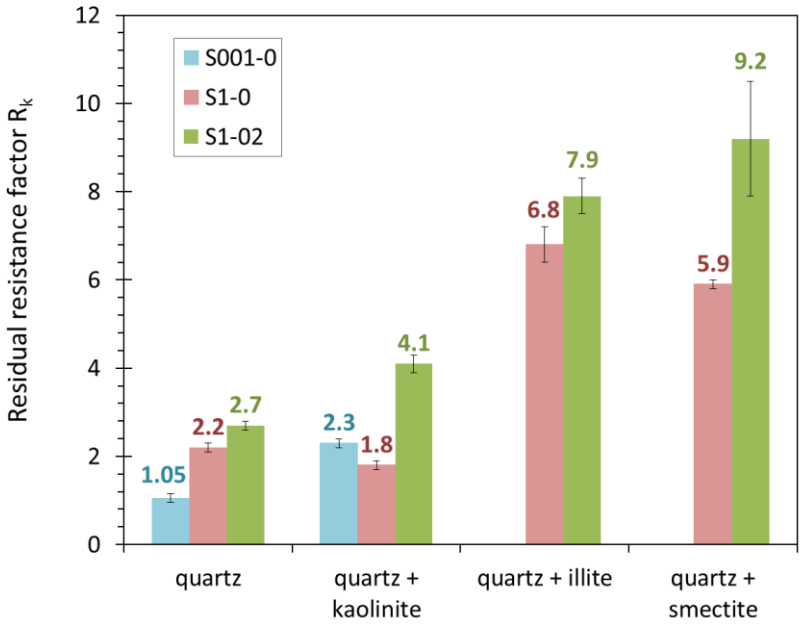

Figure 15: Residual resistance, or permeability reduction factors (R_k) determined for the 4 porous media investigated in the various injection brines.

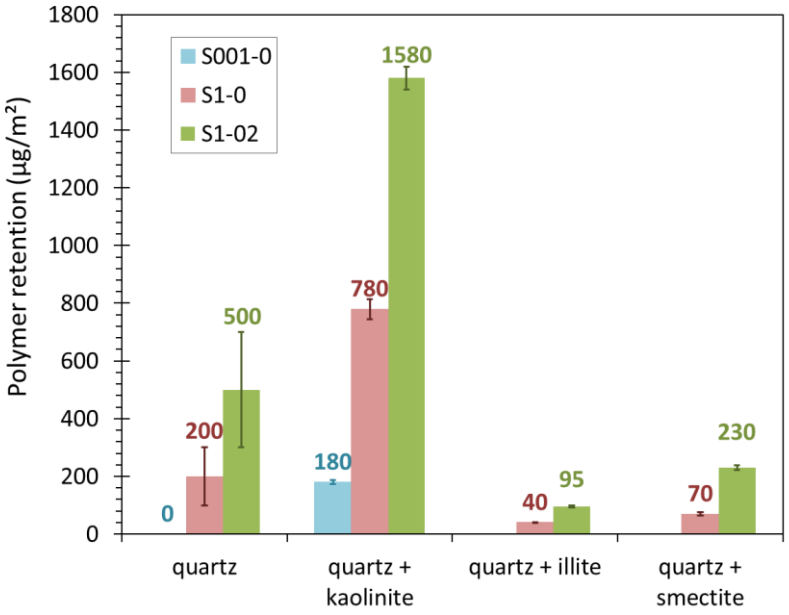

Figure 16: Polymer irreversible retentions (expressed in mass –µg– of retained polymer per unit of measured specific surface area of the sand and clays grains) determined for the 4 porous media investigated in the various injection brines.

Adsorbed layer analysis for the quartz and quartz + kaolinite porous media

In this section, we propose to test the validity of the representation of polymer retention as the creation of a homogenous layer of adsorbed polymer by analyzing the results in terms of adsorbed layer density. From the determination of the irreversible retention per unit surface and of the adsorbed layer thickness, derived from the R_k values (see Eq. 7 and 8), an adsorbed layer density ρ_{ads} can be estimated as follows:

$$\rho_{ads} = \frac{\Gamma_{retention}}{\varepsilon_h} \qquad \text{(Eq.10)}$$

Regarding the quartz porous media, adsorbed layer thicknesses and densities are plotted in Figure 17, for the three injection brines investigated. Apart from the case in which almost no polymer is retained in S001-0, it appears that the adsorbed layer density reaches 550 g/m^3 in S1-0 and 1440 g/m^3 in S1-02 while the thickness remains close to 0.3 µm in both brines. This marked increase of the adsorbed layer's density with hardness can be explained considering the

outcomes of the viscometric and DLS studies (see Table 4 and Figure 9): in the hard brine, intrinsic viscosity is two times less than in the soft brine, which means that the solubilized polymeric objects are denser, while according to DLS they are not smaller in size. This is due to both cationic bridging by Ca^{2+} ions within each macromolecules (intra-chain attractive interactions) and, to some extent, between macromolecules (inter-chains attractive interactions). From these considerations, as schematically presented in Figure 18, it can be understood that a significantly denser polymer adsorbed layer was created when polymer was injected in S1-02 than in S1-0 (because of intra-chain attractive interactions) while having a similar thickness (because of inter-chains attractive interactions). These elements justify the entire adsorbed layer analysis for the quartz porous media. As a result, for this type of porous media, the present study confirms that the polymer is meanly retained by a "fast" mechanism of adsorption at the pore walls, including the pore throats, creating an almost impermeable and homogeneous layer responsible for the permeability reduction.

Regarding the quartz and kaolinite porous media, adsorbed layer thicknesses and densities are plotted in Figure 19 for the three injection brines investigated. Results firstly show that, with increasing ionic strength, adsorbed layer density increases from 620 g/m^3 in S001-0 to 2830 g/m^3 in S1-0, while the adsorbed layer thickness remains close to 0.3 µm. The density variation is consistent with the marked decrease in intrinsic viscosity from S001-0 to S1-0 (classically interpreted as a charge screening effect), but the fact that the thickness remains the same is surprising in view of the DLS results. Indeed, as no mechanisms promoting inter-chains attractive interactions are in play in S1-0, the polymer particles are smaller than in S001-0 and the adsorbed layer should be thinner. When hardness is increased, adsorbed layer density decreases from 2830 g/m^3 to 2060 g/m^3 while the thickness markedly increases from 0.3 µm to 0.75 µm. Such behavior, which is schematically presented on Figure 19, contradicts the outcomes of the viscometric and DLS study and can hence not be interpreted. This means that the adsorbed layer analysis fails for the quartz + kaolinite porous media. As the polymer retention mechanism remains "fast" in these porous media (similar to that in the quartz porous media, according to the R_m vs. number of pore volume injected results, see Figure 12), direct

interactions between polymer and surface could nevertheless still be the main mechanism in play. The fact that providing quantitative data on the polymer adsorbed layer is not possible could be due to the inhomogeneity of the adsorbed layer, originating in the different chemical affinity of the polymer for kaolinite and quartz, respectively.

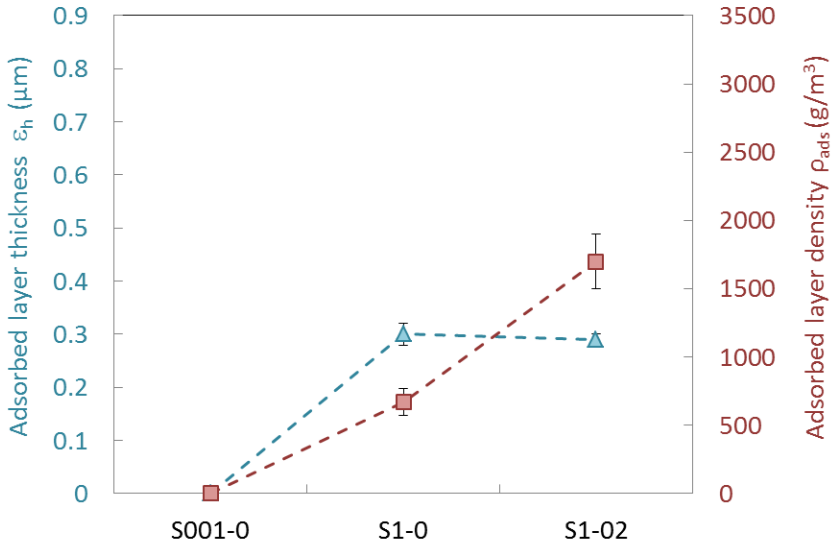

Figure 17: Estimations of the polymer adsorbed layer thicknesses and densities for the tests performed in the quartz porous media for the various salinities investigated.

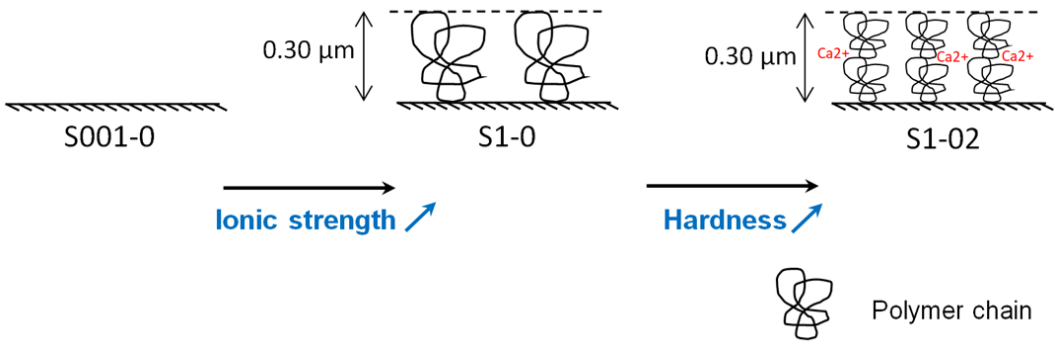

Figure 18: Graphical interpretation of the impact of ionic strength and hardness on the thickness and density of the polymer adsorbed layer in the quartz porous media. For this type of porous media, the adsorbed layer analysis is relevant.

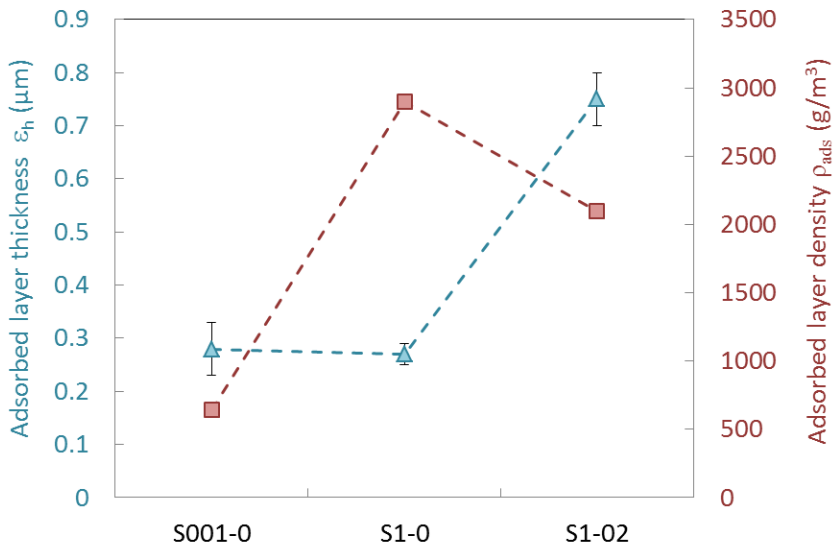

Figure 19: Estimations of the polymer adsorbed layer thicknesses and densities for the tests performed in the quartz + kaolinite porous media for the various salinities investigated.

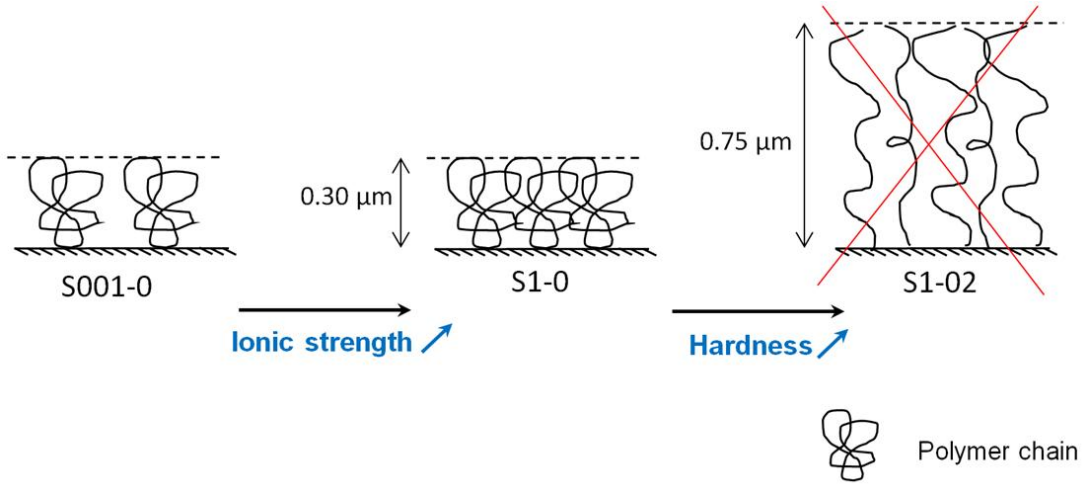

Figure 20: Tentative graphical interpretation of the impact of ionic strength and hardness on the thickness and density of the polymer adsorbed layer in the quartz + kaolinite porous media. For this type of porous media, the adsorbed layer analysis is not relevant.

Textural analysis for the quartz + illite and quartz + smectite porous media

From the experimental results acquired in the present study, the textural analysis proposed for the quartz + illite and quartz + smectite porous media can only be qualitative.

The main elements available from the polymer injection tests are the following: long-term increasing R_m trends, abnormally low retention given the specific surface area and high R_k. From the SEM observations, presented in Table 6 and Table 7, aggregates of illite and smectite as large as the larger quartz grains have clearly been formed in brine. It is clear that these aggregates hold the vast majority of the surface area in their microstructures. A poor penetration of the polymer in the aggregates can hence explain the very low retentions, because it is determined using a technique based on polymer injected volume at breakthrough, hence accounting only for "fast" mechanisms. In this line of interpretation, the slow increasing R_m trends could be the sign of a slow diffusion of the polymer into the aggregates, not accounted for in the retention. This hypothesis is supported by the following observation: R_m curves tend to stabilize slower in the quartz + illite than the quartz + smectite porous media (see Figure 13), whereas the illite aggregates appear denser than that of smectite, on which some porosity appear in the 10 µm-scale enlargement pictures. Both dynamic (coreflood) and static (SEM) results are hence consistent in suggesting that smectite aggregates are more penetrable than illite aggregates.

The high R_k cannot be straightforwardly explained as the available results do not provide information on the microscopic localization of the irreversibly retained polymer. They could be linked to the slow penetration of polymer into the aggregates through polymer accumulation at their outer surface, leading to plugging of some pore throats, hence reducing the permeability.

Overall, in the quartz + illite and quartz + smectite porous media, polymer – surface interaction likely remains the base mechanism, but polymer transport towards adsorption sites is limited by the diffusion of the macromolecules in the illite and smectite aggregates, which is a slow mechanism.

Conclusion

The transport properties of polymer solutions have been studied in controlled and well characterized clayey granular porous media with permeabilities between 50 and 100 mD, having simple mineralogies (quartz only, quartz + kaolinite, quartz + illite and quartz + smectite with 8 wt-% contents in each respective clays) and for various composition of injection brines. Such properties are representative of "low permeability" sandstone reservoir that could be targeted for chemical EOR applications.

The outcomes show that, for clayey porous media, the petrophysical parameters traditionally used to describe polymer transport in porous media (mobility reduction factor, permeability reduction factor and irreversible retention) cannot straightforwardly be interpreted in terms of creation of polymer adsorbed layers, namely:

- for the non-swelling and uncharged clay (kaolinite) polymer transport is easy but involves high retention. Although creation of adsorbed layers is likely to be the main polymer retention mechanism, the layers are heterogeneous;
- for charged or swelling clays (illite and smectite), polymer transport is difficult, but retention not as high as expected. Polymer retention appears governed by diffusion into clays aggregates.

The quantitative results presented in this work can directly be used for forecasting the feasibility of polymer flooding operations in clayey "low" permeability reservoirs, considering the impact of retention on the quality of the in-depth transport on the economics. Further understanding could be achieved byperforming experiments in diluted suspensions, to identify the microscopic polymer-clays interaction and propose a modeling. From a more applied perspective, practical insights could be achieved by applying the experimental methods and interpretation framework proposed in this study on natural clayey porous media.

Acknowledgements

The authors wish to thank IFP Energies nouvelles for funding this work and IFP Energies nouvelles and Université de Lorraine for authorization to publish these results. They are also indebted to Eric Kohler, Joel Lopes De Azevedo and Florent Moreau for the SEM analysis, to Marie-Claude Lynch and Elisabeth Rosenberg for the CT-Scan analysis, to Didier Frot for the DLS experiments, and to Angelina Razafitianamaharavo for gas adsorption experiments..

References

Bagassi, M., Chauveteau, G., Lecourtier, J., Englert, J., Tirrell, M., 1989. Behavior of adsorbed polymer layers in shear and elongational flows. Macromolecules. 22 (1), 262–266. DOI: 10.1021/ma00191a049.

Boujlel, J., Barré, L., Rousseau, D. 2018. New Insights on the Characterization of Polymer Adsorbed Layers in Porous Media. In SPE EOR Conference at Oil and Gas West Asia; Society of Petroleum Engineers, **SPE-190415-MS**.

Brunauer, S., Emmett, P. H., Teller, E. 1938. Adsorption of Gases in Multimolecular Layers. J. Am. Chem. Soc. 60 (2), 309–319. DOI: 10.1021/ja01269a023.

Chauveteau, G. 1981. Molecular Interpretation of Several Different Properties of Flow of Coiled Polymer Solutions Through Porous Media in Oil Recovery Conditions. In SPE Annual Technical Conference and Exhibition. Society of Petroleum Engineers. **SPE-10060-MS**.

Chauveteau, G., Kohler, N. 1974. Polymer Flooding: The Essential Elements for Laboratory Evaluation. In SPE Improved Oil Recovery Symposium. Society of Petroleum Engineers, **SPE-4745-MS**.

Dann, M. W., Burnett, D. B., Hall, L. M. 1982. Polymer Performance in Low Permeability Reservoirs. In SPE Oilfield and Geothermal Chemistry Symposium. Society of Petroleum Engineers, **SPE- 10615-MS**.

Dawson, R., Lantz, R. B. 1972. Inaccessible Pore Volume in Polymer Flooding. Society of Petroleum Engineers Journal, **SPE-3522-PA**, 12 (05), 448–452. DOI: 10.2118/3522-PA.

Delamaide, E., Tabary, R., Rousseau, D. 2014. Chemical EOR in Low Permeability Reservoirs. In SPE EOR Conference at Oil and Gas West Asia. Society of Petroleum Engineers, **SPE-169673-MS**.

Fletcher, A. J. P., Morrison, G. R. 2008. Developing a Chemical EOR Pilot Strategy for a Complex, Low-Permeability Water Flood. In SPE Symposium on Improved Oil Recovery; Society of Petroleum Engineers, **SPE- 112793-MS**.

Green, D. W., Wilhite, G. P. 2018. Enhanced Oil Recovery, 2nd ed. Society of Petroleum Enginners, Richardson, TX.

Lecourtier, J., Chauveteau, G. 1984. Propagation of Polymer Slugs Through Porous Media. In SPE Annual Technical Conference and Exhibition. Society of Petroleum Engineers, **SPE-13034-MS**.

Le Meur, M., Montargès-Pelletier, E., De Bonnefous de Caminel, M., Gley, R., Caillet, C., Waldvogel, Y., Kanbar, H., Razafitianamaharavo, A., Briois, V,, Fonda, E., Ollivi, L., Villiéras, F. Comparison of reactivity and association mode of Zn between natural Suspended Particulate Matter (SPM) and lab controlled particles (in preparation).

Marker, J. M. 1973. Dependence of Polymer Retention on Flow Rate. Journal of Petroleum Technology, **SPE-4423-PA**, 25 (11), 1307–1308. DOI: 10.2118/4423-PA.

Marliere, C., Wartenberg, N., Fleury, M., Tabary, R., Dalmazzone, C., Delamaide, E. 2015. Oil Recovery in Low Permeability Sandstone Reservoirs Using Surfactant-Polymer Flooding. In SPE Latin American and Caribbean Petroleum Engineering Conference. Society of Petroleum Engineers, **SPE- 177072-MS**.

Martin, F. D. 1974. Laboratory investigations in the Use of Polymers in Low Permeability Reservoirs. In Fall Meeting of the Society of Petroleum Engineers of AIME. Society of Petroleum Engineers, **SPE- 5100-MS**.

Mikhail, R.S., Brunauer, S., Bodor, E.E. 1968. Investigations of a complete pore structure analysis. Journal of Colloid and Interface Science. 26 (1), 45–53. DOI: 10.1016/0021-9797(68)90270-1.

Neaman, A., Pelletier, M., Villiéras, F., 2003. The effects of exchanged cation,compression, heating and hydration on textural properties of bulk bentonite andits corresponding purified montmorillonite. Applied Clay Science 22, 153–168.

Pefferkorn, E. 1999. Polyacrylamide at Solid/Liquid Interfaces. Journal of Colloid and Interface Science. 216 (2), 197–220. DOI: 10.1006/jcis.1999.6312.

Russel, W. B., Saville, D. A., Schowalter, W. R. 1989. Colloidal dispersions. Cambridge monographs on mechanics; Cambridge University Press: Cambridge.

Sheng, J. 2011. Modern chemical enhanced oil recovery. Theory and practice. Gulf Professional Pub: Amsterdam, Boston,.

Sorbie, K. S. 1991. Polymer-Improved Oil Recovery. Springer Netherlands: Dordrecht, s.l..

Szabo, M. T. 1975. Laboratory Investigations of Factors Influencing Polymer Flood Performance. Society of Petroleum Engineers Journal, **SPE-4669-PA**, 15 (04), 338–346. DOI: 10.2118/4669-PA.

Treiber, L. E., Yang, S. H. 1986. The Nature of Polymer Plugging and a Wellbore Treatment To Minimize It. In SPE Enhanced Oil Recovery Symposium. Society of Petroleum Engineers, **SPE-14948-MS**.

Vela, S., Peaceman, D. W., Sandvik, E. I. 1976. Evaluation of Polymer Flooding in a Layered Reservoir With Crossflow, Retention, and Degradation. Society of Petroleum Engineers Journal, **SPE-5102-PA**, 1976, 16 (02), 82–96. DOI: 10.2118/5102-PA.

Wang, D., Dong, H., Lv, C., Fu, X., Nie, J. 2009. Review of Practical Experience by Polymer Flooding at Daqing. SPE Reservoir Evaluation & Engineering [Online], **SPE-114342-PA**. 12 (03), 470–476; DOI: 10.2118/114342-PA.

Willhite, G. P.; Dominguez, J. G. 1977. Mechanisms of Polymer Retention in Porous Media. Improved Oil Recovery by Surfactant and Polymer Flooding. Elsevier, 511–554.

Zhang, G., Seright, R. 2014. Effect of Concentration on HPAM Retention in Porous Media. SPE Journal, **SPE-166265-PA**, 19 (03), 373–380. DOI: 10.2118/166265-PA.

Zhang, X., Cresswell, M. 2015. Inorganic Controlled Release Technology. Materials and Concepts for Advanced Drug Formulation; Elsevier Science: Burlington.